

Hidden multiple bond effects in dynamic force spectroscopy

Sebastian Getfert¹ and Peter Reimann
Universität Bielefeld, Fakultät für Physik, 33615 Bielefeld, Germany

¹Corresponding author. Address: Fakultät für Physik, Universität Bielefeld, Universitätsstr. 25, 33615, Bielefeld, Germany. E-Mail: Getfert@Physik.Uni-Bielefeld.De

Abstract

In dynamic force spectroscopy, a (bio-)molecular complex is subjected to a steadily increasing force until the chemical bond breaks. Repeating the same experiment many times results in a broad distribution of rupture forces, whose quantitative interpretation represents a formidable theoretical challenge. In this study we address the situation that more than a single molecular bond is involved in one experimental run, giving rise to multiple rupture events which are even more difficult to analyze and thus are usually eliminated as far as possible from the further evaluation of the experimental data. We develop and numerically solve a detailed model of a complete dynamic force spectroscopy experiment including a possible clustering of molecules on the substrate surface, the formation of bonds, their dissociation under load, and the post processing of the force extension curves. We show that the data, remaining after elimination of obvious multiple rupture events, may still contain a considerable number of “hidden” multiple bonds, which are experimentally indistinguishable from “true” single bonds, but which have considerable effects on the resulting rupture force statistics and its consistent theoretical interpretation.

1 Introduction

The specific binding of a ligand molecule to a receptor protein is an essential functional principle of molecular recognition and information processing in biological systems, e.g. in the context of genome replication and transcription, enzymatic activity, initiation of infection and immune response (1). Furthermore, their force-induced dissociation is of great interest with respect to adhesion and cohesion of any type of biological matter and their selectivity can be exploited in various bioanalytical and biomedical devices (2, 3). The invention and continuous refinement of atomic force microscopy (AFM) and other related techniques (2, 3) has led to a tremendous progress in our abilities to directly investigate such processes on the molecular level (4, 5). Accordingly, dynamic force spectroscopy has become a standard tool in experimental Biophysics to explore and quantify molecular recognition and binding properties of (bio-)molecular complexes, such as reaction off-rates, binding energy landscapes, affinity ranking of single point mutations etc. (1–3). Typical examples include ligand-receptor compounds like antibody-antigen (6), protein-DNA (7), or supramolecular complexes (8). In all these experiments, one of the participating molecules is connected to a tiny force probe and the other to a substrate surface (or an immobilized micron-sized bead). By controlling the relative distance s between these objects with nanometer precision, an experimentally controlled, steadily increasing force $F(s)$ in the Piconewton range can be applied to the compound until the chemical bonds between the constituting molecules rupture, see Fig. 1A.

Repeating the same experiment many times results in a broad distribution of rupture forces, whose interpretation and quantitative analysis represents a formidable theoretical challenge, of foremost importance for our understanding of the basic biophysical principles at work and for the practical evaluation of experimental rupture force data.

In other words, given the distribution of rupture forces for various pulling velocities, a theoretical framework is needed in order to achieve a quantitative characterization of the probed chemical bond in terms of binding affinities, force free dissociation rates, and molecular binding energy landscape parameters. The predominant general framework in this context is due to Evans and Ritchie (9), describing the rupture of a molecular complex as the dissociation of a *single* chemical bond under the externally applied force in terms of a thermally activated escape process with a force dependent decay rate. While Evans and Ritchie adopted the phenomenological approach by Bell (10), important subsequent refinements concern e.g. the specific force dependence of the rate (11–14), multiple dissociation pathways (15), linker

length distributions (16), and contact times (17).

Experimentally, in a given force extension curve $F(s)$ it is often quite obvious that more than one bond has actually been probed (Figs. 1B,C). Since such multiple rupture events cannot be quantitatively evaluated within the above theories, they are usually eliminated as far as possible from the experimental data sets. The key issue of our present work is to take into account the possibility that even after eliminating multiple bonds along this line, the remaining apparent single bonds may in fact still contain a significant number of “hidden” multiple bonds. As we will show, this number is indeed far from negligible under usual experimental conditions. While a recent experimental work has demonstrated that this might indeed be the case (18), a thorough theoretical study of this point has still been missing so far. Such a violation of the basic assumption of the above standard approach in this context is not only of conceptual interest, but also may have considerable practical implications regarding the numerous experimental works employing this “standard” theoretical framework for evaluating their data.

Specifically, within this standard framework the main focus is usually put on the dependence of the most probable rupture force f^* on the pulling velocity v . While the corresponding predictions indeed agree very well with most experiments, a more careful analysis of the complete rupture force distribution reveals that most experimental data are actually incompatible with any of those models (19, 20), in particular the typical “long tails” (17, 18) of the experimental rupture force distributions, as exemplified by Figs. 1E,F.

A first, purely phenomenological explanation of those incompatibilities in terms of bond-heterogeneities was proposed in (20), amounting to a parametric randomization of the force dependent single bond dissociation rates. Our present work provides for the first time a more detailed microscopic foundation of this ansatz, since a mixture of “true” single bonds and undiscovered multiple bonds is similar to a statistical ensemble of formal single bonds with randomized parameters in the force dependent rate (see discussion in Sect. 4.4). While hidden multiple bonds thus seem to play a prominent role in this context, a more detailed analysis, which goes beyond the scope of our present paper, however indicates, that there may well exist additional microscopic mechanisms which also contribute notably to the above mentioned incompatibilities and their explanation in terms of bond-heterogeneities.

Yet another main conclusion of our present paper is that even though a considerable fraction of rupture forces are due to (unresolved) multiple bonds, the rate parameters can still be extracted from the dependence of

the most probable rupture force on the pulling velocity according to the above mentioned single bond theories. In other words, the hidden multiple bonds heavily contribute to the long tails in Figs. 1 (E) and (F), but hardly to the main peaks.

We should emphasize that besides the investigations of ligand-receptor dissociation, the general realm of so-called “dynamic force spectroscopy” also includes the exploration of protein unfolding, unzipping of DNA strands and DNA hairpins, forced rupture of cell adhesion etc., see e.g. (10, 21–24) and further references therein. These quite different experimental set ups often admit a theoretical treatment quite similar to those mentioned above. However, they usually do *not* exhibit any kind of incompatibilities e.g. in the form of long tails, see e.g. (11, 13, 23–28). Our present approach specifically and exclusively concerns the case of “dynamic rupture force spectroscopy” by AFM, micropipette-based force probes, laser tweezers etc. (1–3). With the exception of (29), the problem of the long tails does arise for all those rupture force experiments we know of.

As far as multiple bond models are concerned, we build on several related previous studies: A common starting point in many of those works, see e.g. (10, 21, 22, 30–38), is the assumption that the applied force is equally distributed among all bonds. Closer inspection however shows that the distribution of the rupture forces, expected from these models, in general exhibits, unlike the experimentally observed ones (Figs. 1E,F), several well separated peaks, which are attributed to single, double, triple, ... bonds (34, 38), see also Sect. 4.3 below for more details. In other words, the assumption of equally distributed forces must be given up. Such a refined theoretical treatment has been developed for the first time by Akhremitchev and coworkers (38), but their approach still exhibits several other strong oversimplifications: First, the number of receptors still cannot be more than one, while the number of ligands is at most two. Second, in case of two coexisting bonds, both of them are assumed to rupture simultaneously. Another important series of works considering forces which are unequally distributed among several coexisting bonds is due to Gao and coworkers (39, 40). Formally, they are quite similar to our present study but physically they focus on cell adhesion and do not admit any conclusions with respect to our present case.

Taking into account the very fact that force extension curves with clearly visible multiple bond signatures (Figs. 1B,C) are discarded before further evaluating those data, is yet another essential difference between our present work and all the above mentioned previous multiple bond studies.

Conceptually, the basic idea of our paper is to establish and analyze a

simplified but still reasonably realistic model of the entire experimental procedure: preparation (functionalization) of the AFM tip and of the sample surface; formation of bonds; retraction of the tip from the surface, leading to bond dissociation (rupture events); processing and evaluation of the so obtained data exactly as in the case of real experimental data. The advantage of such a “computer experiment” is that the interpretation of the data and the final conclusions can be immediately compared with what was actually going on in the considered system.

2 Model

2.1 Functionalization of tip and sample

A typical experimental setup we have in mind is exemplified by Fig. 2A. As illustrated by Fig. 2B, the AFM tip is modeled as a half sphere of experimentally realistic radius $R = 15$ nm, to which ligands are connected via linkers of experimentally realistic length $L = 30$ nm. The number of linkers is thus equal to the number of ligands and is denoted by N_{lin} . The vector connecting the tip apex with the immobilization point of linker i ($i = 1 \dots N_{\text{lin}}$) is denoted as $\mathbf{r}_i^{(\text{lin})}$ and the N_{lin} immobilization points themselves are randomly sampled according to a uniform distribution on the half sphere. In a real experiment, the number N_{lin} of linkers attached to the tip is itself a random variable with a distribution which depends in a highly complicated way on the (chemical) functionalization procedure. Within our model, we assume the linker number N_{lin} to be given and we will show that our conclusions concerning, e.g., the distribution of rupture forces, depend very little on the exact value of N_{lin} , at least as long as $N_{\text{lin}} \gtrsim 5$ (see Sect. 3). In view of typical grafting densities of, e.g., the PEG linkers used in (8), a realistic choice which we often adopt in our numerical calculations below is $N_{\text{lin}} = 10$.

The receptors are randomly immobilized on the sample surface with no or negligibly short linkers. Beside the case that they are independently and uniformly distributed according to some preset density ρ_{rec} (Sec. 3), we will also discuss the case that the receptors are distributed in clusters of varying size (Sec. 4).

2.2 Force distance cycle

Usually one refers to a single repetition/run of a pulling experiment as a force distance cycle: In a first step, tip and sample are brought into contact

(at the origin of our coordinate system) for a certain “dwell-time” t_{dwell} (typically 0.1 – 1s), during which receptors and ligands may form bonds. Then, the AFM tip is retracted along the z-axis, $\mathbf{r}_{\text{apex}}(t) = (0, 0, z(t))$ (cf. Fig. 2), resulting in a steadily increasing force on the single bonds until they rupture. In the force extension curve, bond ruptures induce more or less pronounced force dips (Figs. 1A-D). As in the real experiment, if more than one such dip is clearly visible (Figs. 1B,C), the corresponding force extension curve is discarded.

Before discussing these steps in more detail in the following subsections, we remark that while the AFM tip and thus the linker immobilization points $\mathbf{r}_i^{(\text{lin})}$ remain the same for all cycles (see Fig. 2B), a new random sampling of the receptor positions will be performed for each cycle, modeling the fact that in a real experiment the sample surface is usually “scanned” either due to thermal drift or controlled lateral displacements.

2.3 Formation of bonds

We consider N_{lin} ligands, attached by linkers to the AFM tip, and a surface with randomly distributed receptors, having the opportunity to form bonds during the dwell time t_{dwell} . The resulting number of bonds thus depends on the dynamics of a nanometer-sized object tethered to a polymer chain, which itself may interact with other chains, and which is subjected to complicated boundary conditions (half-sphere on a flat surface) and far from equilibrium initial conditions. Instead of theoretically addressing this very difficult problem, we invoke the experimental findings in a related situation, namely the association of end-grafted chains to uniformly reactive surfaces (41–43). As a result of these works, the probability that a bond between a tethered molecule and one of its potential binding partners at a distance d is actually formed is approximately constant for $d < d_{\text{max}}$ and negligible for $d > d_{\text{max}}$, where $d_{\text{max}} \approx 10\text{-}15$ nm for PEG linkers with $L \approx 30$ nm and $t_{\text{dwell}} \approx 1$ s. Moreover, the number of remaining “unpaired potential binding partners” closer than d_{max} is relatively small.

We therefore proceed as follows: First, all ligand-receptor pairs with a distance smaller than d_{max} are identified. Then, one of these pairs is randomly chosen to form a bond. For the remaining receptors and ligands these two steps are repeated, until no pair with a distance smaller than d_{max} is left. The total number of the so obtained bonds is henceforth denoted as N . In our numerical calculation below, our standard choice will be $d_{\text{max}} = 12$ nm, while a more detailed exploration of other choices will be discussed in Sect. 4.3.

We have also tried out other strategies for the bond formation, for example that a ligand preferentially forms a bond with the closest receptor. This, however, yielded very similar results to the above mentioned procedure.

2.4 Force extension curves

Denoting by $\mathbf{r}_i^{(\text{lin})}$ and $\mathbf{r}_i^{(\text{rec})}$ the linker and receptor immobilization points of the i -th bond ($i = 1 \dots N$), the linker's end-to-end vector is (see Fig. 2B)

$$\mathbf{r}_i = z\mathbf{e}_z + \mathbf{r}_i^{(\text{lin})} - \mathbf{r}_i^{(\text{rec})} = l_i \hat{\mathbf{r}}_i, \quad (1)$$

where \mathbf{e}_z is the unit vector in z -direction, $\hat{\mathbf{r}}_i$ is the unit vector in \mathbf{r}_i -direction, and l_i is the length (modulus) of $\mathbf{r}_i(z)$.

Due to entropic effects, stretching the linker to a length l_i requires a force of modulus f_i which acts in the direction of the end-to-end vector, i.e.

$$\mathbf{f}_i = f_i \hat{\mathbf{r}}_i. \quad (2)$$

A particularly simple model for this force-dependence of the linker length is the freely jointed chain (FJC) model, according to which

$$l_i(f_i) = L \left[\coth \left(\frac{\lambda_K f_i}{k_B T} \right) - \frac{k_B T}{\lambda_K f_i} \right], \quad (3)$$

where λ_K is the Kuhn length and $k_B T$ the thermal energy. As a typical value, obtained by stretching experiments on PEG linkers at room temperature (2), we employ $k_B T / \lambda_K = 6$ pN. Numerically inverting Eq. 3 then yields the force extension characteristic $f_i(l_i)$ of a single linker which we henceforth will utilize in our model.

For the pulling geometries studied in our present work, the experimentally accessible observable is not the magnitude of the total force $\mathbf{F} = \sum_{i=1}^N \mathbf{f}_i$, but rather it's normal component with respect to the sample surface (44), i.e.

$$F := \mathbf{F} \cdot \mathbf{e}_z = \sum_{i=1}^N (\hat{\mathbf{r}}_i \cdot \mathbf{e}_z) f_i. \quad (4)$$

A priori, all quantities in Eqs. 1-4 are functions of z . However, the actual control parameter in the experiment is the displacement

$$s = vt \quad (5)$$

of the sample surface from its initial position, with a typical experimental pulling velocity $v = 1000$ nm/s. Furthermore, the displacement s can be

written as the sum of z and the deflection of the cantilever under the force F , i.e.

$$s = z + F/\kappa , \quad (6)$$

with a typical experimental cantilever stiffness (2) of $\kappa = 10$ pN/nm. Via Eq. 6, all the above quantities, in particular the force F from Eq. 4, may thus alternatively be expressed as functions of s , and likewise, via Eq. 5, as functions of t . In the following, we will switch between these alternatives without much further ado. In particular, $F(s)$, following from Eq. 4 with s as independent variable, is called the force extension curve.

2.5 Rupture probabilities

For an arbitrary but fixed bond i , the force f_i appearing in Eq. 4 follows by inverting 3 before the bond has ruptured and is given by $f_i = 0$ after rupture. According to Evans and Ritchie (9), the rupture process itself is a thermally activated rate process, governed by

$$\dot{n}_i(t) = -k(f_i(t))n_i(t), \quad n_i(t=0) = 1 , \quad (7)$$

where $n_i(t)$ denotes the survival probability of the bond up to time t , and $k(f_i(t))$ is the force dependent bond-dissociation rate. Consequently,

$$n_i(t) = \exp \left[- \int_0^t dt' k(f_i(t')) \right] \quad (8)$$

and the probability of bond rupture then follows as $-dn_i(t)/dt$. Denoting by $t_i(f)$ the inverse of the function $f_i(t)$, one furthermore obtains the survival probability $n_i(f) := n_i(t_i(f))$ of the i -th bond as a function of the instantaneous force f acting on that bond.

In our quantitative calculations below, we will adopt the simplest and most common approximation (10)

$$k(f) = k_0 \exp(x_b f / k_B T) , \quad (9)$$

where k_0 is the force-free dissociation rate and x_b the distance between potential minimum and barrier along the direction of the applied force. Furthermore, we will use the following typical values of those rate parameters:

$$k_0 = 0.1 \text{ s}^{-1} , \quad x_b / k_B T = 0.1 \text{ pN}^{-1} . \quad (10)$$

We remark that the alternative approximations for $k(f)$ from (14) did not lead to notably different findings than Eq. 9.

2.6 Simulation and processing of force extension curves

The initial condition in the form of N bonds at time $t = 0$ is set according to Sect. 2.3. For the further time evolution we adopt – similarly as in (21, 22, 39, 40) – Gillespie’s algorithm (45) with time-dependent forces and rupture probabilities as detailed in Sects. 2.4 and 2.5, respectively.

Fig. 3 exemplifies six force extension curves simulated along these lines. They indeed look quite similar to the experimental curves from Figs. 1A-D. In particular, while in the left panels of Fig. 3 the two rupture events (“dips” or “jumps”) happen to be well separated, the two bonds accidentally rupture nearly simultaneously in the right panels. In the middle panels, the rupture of the first bond happens to be still visible as a small force dip, but due to the limited resolution of a real experimental device (cf. Fig. 1D), it is questionable whether in practice such a force signal could be distinguished from that of a single bond.

For comparison, the bottom right panel in Fig. 3 also shows a typical force extension curve from a “numerical experiment” with a single bond ($N = 1$). This example corresponds to the more likely situation that the single bond ruptures earlier than the two bonds, but since these are random events with a quite broad distribution (see later sections), it might also be the other way round with quite some probability. Within the experimentally realistic noise level which has been used for the illustration in Fig. 3, it thus is indeed practically impossible to tell on the basis of the dotted and the solid lines in the right and middle panels of Fig. 3, which one was originally due to a double and a single bond, respectively.

Similar observations apply to more than two bonds. In other words, it seems reasonable to assume that the rupture of a multiple bond complex cannot be distinguished from that of a single bond if all bonds rupture within some small distance Δs_{\max} . In view of Figs. 1A-D and 3, $\Delta s_{\max} = 1$ nm seems to be an optimistic but still reasonable choice for the resolution limit, in good agreement with the experimental value of $\Delta s_{\max} \approx 4$ nm reported in (18) for relatively long linkers. A more detailed discussion of the specific choice of Δs_{\max} will be provided in Sect. 4.3.

A further consequence of the instrumental noise is that only rupture forces beyond some threshold value f_{\min} can be clearly distinguished from the noise. In our numerical examples below, we will always adopt the experimentally realistic choice $f_{\min} = 20$ pN since we found that any other choice of f_{\min} within reasonable limits (say between 0 pN and 40 pN) hardly affected the results with the obvious exception of different “lower cutoffs” in rupture force histograms like Figs. 1E,F.

As in real experiments, force extension curves which exhibit clearly resolvable signatures of multiple bonds are excluded from the further analysis. In turn, this means that force extension curves of multiple bonds will still be accepted if all bonds with rupture force larger than f_{\min} rupture within a distance Δs_{\max} . Such multiple bonds, which are erroneously classified as single bonds will henceforth be denoted as “false single bonds” or “hidden multiple bonds”. In turn, both the “true” and “false” single bonds will be called “apparent single bonds”. The force value, at which an apparent single bond ruptures is defined by the maximum of the force extension curve $F(s)$, is termed “rupture force”, and is conventionally denoted by the letter f . Due to the random features of tip functionalization (Sect. 2.1), bond formation (Sect. 2.3), and bond rupture (Sects. 2.5 and 2.6), the rupture force f is a random variable, whose probability density is henceforth denoted as $p(f)$.

3 Uniformly distributed receptors

For a uniform receptor density ρ_{rec} (cf. Sect. 2.1), the number of receptors on a surface area A is a Poisson distributed random number with mean value $\rho_{\text{rec}}A$. Sampling receptors along these lines, we simulated a number of force distance cycles so that 1000 of them were exhibiting at least one rupture event (i.e. $N \geq 1$). In Figs. 4A,B we moreover averaged over 100 different AFM tips (cf. Sect. 2.1), while Figs. 4C,D depict representative results for one single tip.

The blue line in Fig. 4A shows that the probability of classifying an actual multiple bond as an apparent single bond is 40-50% and decreases only weakly with increasing density ρ_{rec} of receptors. Likewise, the fraction of “hidden multiple bonds” among all apparent single bonds (black line in Fig. 4A) increases remarkably fast as a function of ρ_{rec} . However, for these ρ_{rec} values, also the probability to observe at least one rupture event during one force distance cycle (red line in Fig. 4A) is quite large compared to the usual experimental findings. We come back to this point in Sec. 4.1.

Fig. 4B shows that the rupture force, averaged over all apparent single bonds, exhibits a moderately increasing behavior as a function of the receptor density ρ_{rec} . This finding is quite plausible in view of the increasing number of hidden multiple bonds, which are expected to rupture on the average at higher force values than the true single bonds.

For small receptor densities ρ_{rec} , almost only true single bonds contribute to the distribution of rupture forces $p(f)$ which is consequently sharply peaked and exhibits a fast decay for large f (Fig. 4C). For higher receptor

densities, the distribution of rupture forces develops a long tail (Fig. 4D) due to the increasing fraction of hidden multiple bonds, much like for the real data exemplified by Figs. 1E,F. Interestingly, the distribution still exhibits a pronounced peak which (by comparison to Fig. 4C) is mainly caused by the rupture events of the true single bonds, while no distinct additional peaks due to double and more general multiple bonds are visible.

While Fig. 4 was obtained for AFM tips with $N_{\text{lin}} = 10$ linkers, Fig. 5 shows that $N_{\text{lin}} = 5$ and $N_{\text{lin}} = 15$ lead only to minor changes of these results.

4 Clustering of receptors

4.1 Motivation

Experimentally, the receptor density is controlled via the chemical preparation procedure of the sample surface. Usually it is adjusted such that the probability to observe at least one rupture event during one force distance cycle (red lines in Figs. 4 and 5) is quite low (typically below 20%). Assuming a uniform distribution of receptors on the surface, the probability of multiple bonds would then be negligibly small, cf. Figs. 4 and 5. It can be shown that this observation is largely independent of the remaining model parameters and does also apply to other geometries of the AFM tip. Yet, in real experiments multiple bonds are actually observed at a much higher rate. This seems to us a quite convincing direct evidence that the receptors are in fact not uniformly distributed on the surface. Physical reasons of why the density of receptors may be *locally* considerably larger than on the average are: (i) The receptors (or the linkers used to immobilize them on the substrate) may tend to cluster due to mutual interactions, insufficient mixing or substrate inhomogeneities (some areas may be more “reactive” than others). (ii) One receptor may exhibit several identical binding sites for the ligand, like e.g., streptavidin for biotin (38).

4.2 Modeling

Receptor clusters are uniformly distributed on the sample surface according to some cluster density ρ_{clu} . For any given cluster, the number of receptors N_{clu} , is sampled from a Poisson distribution with mean $\langle N_{\text{clu}} \rangle$ and the receptors are then independently distributed within a circle of radius $R_{\text{clu}} = 2$ nm. Other values of R_{clu} lead to very similar results, as long as they remain smaller than the maximal binding length d_{max} (cf. Sect. 2.3). Likewise, we

will always focus on the specific cluster density $\rho_{\text{clu}} = 10^{-4} \text{ nm}^{-2}$ since the value of ρ_{clu} is in fact irrelevant as long as multiple bonds involving receptors from different clusters are negligible. Finally, we restrict ourselves to average cluster sizes $\langle N_{\text{clu}} \rangle = 2$ and discuss the influence of the parameters d_{max} and Δs_{max} in some more detail.

4.3 Results

Fig. 6 shows numerical results for different values of the maximal binding length d_{max} . Proceeding as detailed in Sects. 2 and 4.2, we simulated a number of force distance cycles so that 10000 of them were exhibiting at least one rupture event (i.e. $N \geq 1$), but unlike in Sect. 3, no additional sampling over different AFM tips was performed. The resulting probabilities of observing at least one rupture event during a force distance cycle were approximately 5% for $d_{\text{max}} = 8 \text{ nm}$, 11% for $d_{\text{max}} = 12 \text{ nm}$, and 17% for $d_{\text{max}} = 16 \text{ nm}$. As mentioned in Sect. 4.1, these are typical values for real experiments.

Since resolution limits $\Delta s_{\text{max}} \lesssim 1 \text{ nm}$ seem to be experimentally unrealistic (cf. Figs. 1A-D, 3), Fig. 6A implies that a large fraction of actual multiple bonds will be classified as apparent single bonds, and Fig. 6B shows that a considerable fraction of apparent single bonds are actually multiple bonds.

Also the rupture force distributions $p(f)$ (Fig. 6C) seem to depend only quite weakly on the maximal binding length d_{max} , apart from two details: (i) In contrast to Fig. 4D, the rupture force distributions develop a small secondary peak upon decreasing d_{max} . The reason is that for small d_{max} , the force is always more or less equally distributed among the multiple bonds, giving rise to well separated peaks for single, double, triple, ... bonds. With increasing d_{max} values, multiple bonds with unequally distributed forces become more likely, hence the force peaks are smeared out and finally disappear. In either case, it is questionable whether the minima of the rupture force distributions $p(f)$ in Fig. 6C can also be resolved in practice, where sample sizes are in general much smaller (see also Figs. 1E,F and 7A-D) and where the peaks are broadened by noise. (ii) The complete rupture force distribution $p(f)$ for $d_{\text{max}} = 16 \text{ nm}$ is slightly shifted towards lower forces compared to the distribution for $d_{\text{max}} = 8 \text{ nm}$. The reason is that the rupture force corresponds to the force measured by the AFM cantilever and not to the force acting on the bond, see Fig. 2B. For larger values of d_{max} it is more probable that one is pulling under a large angle relative to the surface normal (see Fig. 2B), resulting in smaller values of the measured

rupture forces.

4.4 Variations of the pulling velocity

Fig. 7 shows the numerical imitation of a complete dynamic force spectroscopy experiment: For each pulling velocity v we simulated 500 force distance cycles as detailed in the preceding sections, employing $d_{max} = 12$ nm, $\Delta s_{max} = 1$ nm, and the same AFM tip as in Fig. 6. The resulting probabilities of observing at least one rupture event during a force distance cycle were approximately 10% for all pulling velocities v .

While a detailed quantitative comparison/fitting with any specific experiment is not the purpose of our present paper, the general similarity between the typical experimental data from Figs. 1E,F and the numerical simulations in Figs. 7A-D is quite convincing. In particular, we recover the typical “long tails” announced in Sect. 1.

For a given pulling velocity v , the survival probability $n(f)$ of the apparent (“true” or “false”) single bonds readily follows from the rupture force distribution $p(f)$ according to

$$n(f) = \int_f^\infty p(f') df' . \quad (11)$$

Fig. 7E presents those survival probabilities for various pulling velocities v . As demonstrated in (20), all these functions $-v \ln p(f)$ must collapse onto a single, v -independent “master curve” in the absence of false single bonds, while experimentally they actually split in a very similar way to the curves shown in Fig. 7E. In (20) this was explained by adopting a parametric randomization of the dissociation rate from Eq. 9. In our case, the dissociation rate for a single bond i can be written as $k_0 \exp[(x_b a_i)F/k_B T]$ where $a_i := f_i/F$. For a fixed force F , a_i is a random variable depending on the number of parallel bonds and their configuration. Effectively, hidden multiple bonds thus result in very similar rupture force distributions as bond heterogeneities.

The fact that the curves in Fig. 7E indeed do collapse onto a single master curve for small f -values further corroborates the above discussed implications of Figs. 4 C and D, namely that the hidden multiple bonds mainly affect the rupture force distribution beyond its maximum, while the maximum itself is mainly governed by the “true” single bonds.

4.5 Most probable rupture forces

As seen above, hidden multiple bonds hardly affect the maximum of the rupture force distribution. In other words, the most probable rupture force f^* admits an adequate and consistent theoretical treatment within the “traditional” single bond picture by Evans and Ritchie (9), cf. Sect. 1. In particular, the rate parameters $x_b/k_B T$ and k_0 appearing in Eq. 10 can still be estimated by plotting f^* versus $\ln \lambda$ due to the well established relation

$$f^* = (k_B T/x_b) \ln (x_b \lambda/k_B T k_0) \quad (12)$$

where $\lambda := F'(s(f^*))v$ is the so-called loading rate (9).

Fig. 7F confirms that the most probable rupture force resulting from our simulations indeed depends linearly on $\ln \lambda$. By fitting a straight line through these points one recovers by means of Eq. 12 the following estimates

$$k_0 = 0.17 \text{ s}^{-1} , \quad x_b/k_B T = 0.0989 \text{ pN}^{-1} , \quad (13)$$

in good agreement with the original, “true” rate parameters from Eq. 10.

5 Discussion

By a detailed modeling and simulation of a complete dynamic force spectroscopy experiment – including the formation of bonds, their dissociation under load, and the post processing of the force extension curves – we have shown that multiple bonds cannot be detected with sufficient reliability on the basis of the experimentally accessible information, namely force extension curves exhibiting several distinct force dips (Figs. 1A-D, 3). In particular, in order to explain the typical experimentally observed frequencies of force distance cycles exhibiting zero, one, and more than one rupture events, we found that assuming some kind of receptor and/or linker clustering seems unavoidable (Sect. 4.1). As a consequence, a quite reliable indicator that a significant number of multiple bonds are misinterpreted as single bonds is a non-negligible fraction of force extension curves with experimentally resolvable multiple dips.

For the sake of simplicity, we have assumed that the receptors are immobilized directly on the substrate and that the ligands are connected to the AFM tip via linkers of fixed length. Under typical experimental conditions, about half of the multiple rupture events then turned out to be undetectable, largely independent of the association dynamics and other details of the modeling. Cases when both, receptors and ligands are immobilized

via linkers, which may furthermore exhibit a broad length distribution, are considerably more difficult to model (46), but intuitively we still expect comparable fractions of hidden multiple bonds, in good agreement with recent experimental observations (18).

A somewhat related problem in the context of protein unfolding has recently been addressed by Dietz and Rief (47). These authors have connected the protein of interest to a modular protein chain resulting in characteristic sawtooth patterns in the force extension curves. Employing an objective pattern recognition algorithm, Dietz and Rief then used these “fingerprints” to identify the “true” single molecule unfolding events. Similar experimental and theoretical attempts in case of dynamic force spectroscopy are not known to the present authors. But at least we can provide a way to “live” with those apparently unavoidable “hidden” multiple bonds, namely by focusing on the most probable rupture force and disregarding the “long tails” of the full rupture force distribution. In other words, our work provides a solid justification of what many experimentalists have always been doing anyway. Finally, Zhu and coworkers (48) have pointed out already in 1998 that it is possible to discern single from multiple bonds in micropipette measurements just by visually monitoring the detachment of the cell. They further showed, that by varying the waiting time for bond formation, it is possible to extract the kinetic rates and the mean number of bonds. This however required a precise control of the density and distribution of receptors and ligands, as well as a correct stochastic description of the association process. Analogous options in the case of measurements by AFM, where this is not available (see Sects. 2.3 and 4.1), are not known to us.

Acknowledgments

Special thanks is due to D. Anselmetti and A. Bieker for providing the data presented in Fig. 1. We also thank A. Fuhrmann, R. Ros, and V. Walhorn for helpful discussion. Financial support by the Deutsche Forschungsgemeinschaft within the Collaborative Research Center SFB 613 is gratefully acknowledged.

References

- [1] Hinterdorfer, P., and Y. F. Dufrene. 2006. Detection and localization of single molecular recognition events using atomic force microscopy. *Nat. Methods* 5:347-355.

- [2] Merkel R. 2001. Force spectroscopy on single passive biomolecules and single biomolecular bonds. *Phys. Rep.* 346:343-385.
- [3] Ritort, F. 2006. Single-molecule experiments in biological physics: methods and applications. *J. Phys.: Condens. Matter* 18:R531-R583.
- [4] Florin, E.-L., V. T. Moy, and H. E. Gaub. 1994. Adhesion forces between individual ligand-receptor pairs. *Science* 264:415-417.
- [5] Dammer, U., M. Hegner, D. Anselmetti, P. Wagner, M. Dreier, W. Huber, and H.-J. Güntherodt. 1996. Specific antigen/antibody interaction measured by force microscopy. *Biophys. J.* 70:2437-2441.
- [6] Hinterdorfer, P., W. Baumgartner, H. J. Gruber, K. Schilcher, and H. Schindler. 1996. Detection and localization of individual antibody-antigen recognition events by atomic force microscopy. *Proc. Natl. Acad. Sci. USA* 93:3477-3481.
- [7] Eckel, R., S.-D. Wilking, A. Becker, N. Sewald, R. Ros, and D. Anselmetti. 2005. Single-Molecule Experiments in Synthetic Biology – An Approach to the Affinity Ranking of DNA-Binding Peptides. *Angew. Chem. Int. Ed. Engl.* 44:3921-3924.
- [8] Schröder, T., T. Geisler, V. Walhorn, B. Schnatwinkel, D. Anselmetti, and J. Mattay. 2010. Single-molecule force spectroscopy of supramolecular heterodimeric capsules. *Phys. Chem. Chem. Phys.* 12:10981-10987.
- [9] Evans, E., and K. Ritchie. 1997. Dynamic Strength of Molecular Adhesion Bonds. *Biophys. J.* 72:1541-1555.
- [10] Bell, G. I. 1978. Models for the Specific Adhesion of Cells to Cells. *Science* 200:618-627.
- [11] Hummer, G., and A. Szabo. 2003. Kinetics from Nonequilibrium Single-Molecule Pulling Experiments. *Biophys. J.* 85:5-15.
- [12] Hanke, F., and H. J. Kreuzer. 2006. Breaking bonds in the atomic force microscope: Theory and analysis. *Phys. Rev. E* 74:031909.
- [13] Schlierf, M., and M. Rief. 2006. Single-Molecule Unfolding Force Distributions Reveal a Funnel-Shaped Energy Landscape. *Biophys. J.* 90:L33-L35.

- [14] Dudko, O. K., G. Hummer, and A. Szabo. 2006. Intrinsic Rates and Activation Free Energies from Single-Molecule Pulling Experiments. *Phys. Rev. Lett.* 96:108101.
- [15] Bartolo, D., I. Derenyi, and A. Ajdari. 2002. Dynamic response of adhesion complexes: Beyond the single-path picture. *Phys. Rev. E* 65:051910.
- [16] Friedsam, C., A. K. Wehle, F. Kühner, and H. E. Gaub. 2003. Dynamic single-molecule force spectroscopy: bond rupture analysis with variable spacer length. *J. Phys.: Condens. Matter* 15:S1709-S1723.
- [17] Lü, S., Z. Ye, C. Zhu, and M. Long. 2006. Quantifying the effects of contact duration, loading rate, and approach velocity on P-selectin-PSGL-1 interactions using AFM. *Polymer* 47:2539-2547.
- [18] Mayyas, E., M. Bernardo, L. Runyan, A. Sohail, V. Subba-Rao, M. Pantea, R. Fridman, and P. M. Hoffmann. 2010. Dissociation Kinetics of an EnzymeInhibitor System Using Single-Molecule Force Measurements. *Biomacromolecules* 11:3352-3358.
- [19] Imparato, A., and L. Peliti. 2004. Kinetic barriers in RNA unzipping. *Eur. Phys. J. B* 39:357-363.
- [20] Raible, M., M. Evstigneev, F. W. Bartels, R. Eckel, M. Nguyen-Duong, R. Merkel, R. Ros, D. Anselmetti, and P. Reimann. 2006. Theoretical Analysis of Single-Molecule Force Spectroscopy Experiments: Heterogeneity of Chemical Bonds. *Biophys. J.* 90:3851-3864.
- [21] Erdmann, T., and U. S. Schwarz. 2004. Adhesion clusters under shared linear loading: a stochastic analysis. *Europhys. Lett.* 66:603-609.
- [22] Erdmann, T., and U. S. Schwarz. 2007. Impact of receptor-ligand distance on adhesion cluster stability. *Eur. Phys. J. E* 22:123-137.
- [23] Dudko, O. K., J. Mathé, A. Szabo, A. Meller, and G. Hummer. 2007. Extracting kinetics from single-molecule force spectroscopy: nanopore unzipping of DNA hairpins. *Biophys. J.* 92:4188-4195.
- [24] Dudko, O. K., G. Hummer, and A. Szabo. 2008. Theory, analysis, and interpretation of single-molecule force spectroscopy experiments. *Proc. Natl. Acad. Sci. USA* 105:15755-15760.

- [25] Li, H., A. F. Oberhauser, S. B. Fowler, J. Clarke, and J. M. Fernandez. 2000. Atomic force microscopy reveals the mechanical design of a modular protein. *Proc. Natl. Acad. Sci. USA* 97:6527-6531.
- [26] Williams, P. M., S. B. Fowler, R. B. Best, J. L. Toca-Herrera, K. A. Scott, A. Steward, and J. Clarke. 2003. Hidden complexity in the mechanical properties of titin. *Nature* 422:446-449.
- [27] Koch, S. J., and M. D. Wang. 2003. Dynamic force spectroscopy of protein-DNA interactions by unzipping DNA. *Phys. Rev. Lett.* 91:028103.
- [28] Dietz, H., F. Berkemeier, M. Bertz, and M. Rief. 2006. Anisotropic deformation response of single protein molecules. *Proc. Natl. Acad. Sci. USA* 103:12724-12728.
- [29] Morfill, J., K. Blank, C. Zahnd, B. Luginbühl, F. Kühner, K.-E. Gottschalk, A. Plückthun, and H. E. Gaub. 2007. Affinity-matured recombinant antibody fragments analyzed by single-molecule force spectroscopy. *Biophys. J.* 93:3583-3590.
- [30] Seifert, U. 2000. Rupture of Multiple Parallel Molecular Bonds under Dynamic Loading. *Phys. Rev. Lett.* 84:2750-2753.
- [31] Evans, E. 2001. Probing the relation between force – lifetime – and chemistry in single molecular bonds. *Annu. Rev. Biophys. Biomol. Struct.* 30:105-128.
- [32] Gergely, C., J. Hemmerle, P. Schaaf, J. K. Heinrich Hörber, J. C. Voegel, and B. Senger. 2002. Multi-Bead-and-Spring Model to Interpret Protein Detachment Studied by AFM Force Spectroscopy. *Biophys. J.* 83:706-722.
- [33] Williams, P. M. 2003. Analytical descriptions of dynamic force spectroscopy: behaviour of multiple connections. *Anal. Chim. Acta* 479:107-115.
- [34] Ratto, T. V., R. E. Rudd, K. C. Langry, R. L. Balhorn, and M. W. McElfresh. 2006. Nonlinearly Additive Forces in Multivalent Ligand Binding to a Single Protein Revealed with Force Spectroscopy. *Langmuir* 22:1749-1757.
- [35] Sulchek, T., R. W. Friddle, and A. Noy. 2006. Strength of Multiple Parallel Biological Bonds. *Biophys. J.* 90:4686-4691.

- [36] Erdmann, T., W. Pierrat, P. Nassoy, and U. S. Schwarz. 2008. Dynamic force spectroscopy on multiple bonds: Experiments and model. *EPL* 81:48001.
- [37] Rankl, C., F. Kienberger, L. Wildling, J. Wruss, H. J. Gruber, D. Blaas, and P. Hinterdorfer. 2008. Multiple receptors involved in human rhinovirus attachment to live cells. *Proc. Natl. Acad. Sci. USA* 105:17778-17783.
- [38] Gu, C., A. Kirkpatrick, C. Ray, S. Guo, and B. B. Akhremitchev. 2008. Effects of Multiple-Bond Ruptures in Force Spectroscopy Measurements of Interactions between Fullerene C₆₀ Molecules in Water. *J. Phys. Chem. C* 112:5085-5092; Guo, S., C. Ray, A. Kirkpatrick, N. Lad, and B. B. Akhremitchev. 2008. Effects of Multiple-Bond Ruptures on Kinetic Parameters Extracted from Force Spectroscopy Measurements: Revisiting Biotin-Streptavidin Interactions. *Biophys. J.* 95:3964-3976.
- [39] Qian, J., J. Wang, and H. Gao. 2008. Lifetime and strength of adhesive molecular bond clusters between elastic media. *Langmuir* 24:1262-1279.
- [40] Chen, B., and H. Gao. 2010. Mechanical principle of enhancing cell-substrate adhesion via pre-tension in the cytoskeleton. *Biophys. J.* 98:2154-2162.
- [41] Jeppesen, C., J. Y. Wong, T. L. Kuhl, J. N. Israelachvili, N. Mullah, S. Zalipsky, and C. M. Marques. 2001. Impact of Polymer Tether Length on Multiple Ligand-Receptor Bond Formation. *Science* 293:465-468.
- [42] Abbou, J., A. Anne, and C. Demaille. 2006. Accessing the Dynamics of End-Grafted Flexible Polymer Chains by Atomic Force-Electrochemical Microscopy. Theoretical Modeling of the Approach Curves by the Elastic Bounded Diffusion Model and Monte Carlo Simulations. Evidence for Compression-Induced Lateral Chain Escape. *J. Chem. Phys.* 110:22664-22675.
- [43] Guo, S., N. Lad, C. Ray, and B. B. Akhremitchev. 2009. Association Kinetics from Single Molecule Force Spectroscopy Measurements. *Biophys. J.* 96:3412-3422.
- [44] Kühner, F., M. Erdmann, and H. E. Gaub. 2006. Scaling Exponent and Kuhn Length of Pinned Polymers by Single Molecule Force Spectroscopy. *Phys. Rev. Lett.* 97:218301.

- [45] Gillespie, D. T. 1977. Exact stochastic simulation of coupled chemical reactions. *J. Phys. Chem.* 81:2340-2361.
- [46] Bubis, R., Y. Kantor, and M. Kardar. 2009. Configurations of polymers attached to probes. *EPL* 88:48001.
- [47] Dietz, H., and M. Rief. 2007. Detecting molecular fingerprints in single molecule force spectroscopy using pattern recognition. *Jpn. J. Appl. Phys.* 46:5540-5542.
- [48] Chesla, S. E., P. Selvaraj, and C. Zhu. 1998. Measuring two-dimensional receptor-ligand binding kinetics by micropipette. *Biophys. J.* 75:1553-1572.

Figure Legends:

Figure 1:

(A)-(D) Typical force extension curves from four “single runs” of a dynamic force spectroscopy experiment by AFM. Ideally, the force $F(s)$ steadily grows with increasing distance s until the chemical bond ruptures (A). In (B) and (C) more than one force dip (“downward jump” of $F(s)$) is clearly visible, indicating that more than a single bond was involved. Curves like in (D) would commonly still be attributed to a single bond rupture within the given noise level and resolution limit. The depicted experimental data in (A)-(D) for a protein-DNA complex (PhoB mutant and target sequence, pulling velocity of 2000 nm/s, cantilever stiffness 13 pN/nm, linker length 30 nm) have been kindly provided by A. Bieker and D. Anselmetti (Bielefeld University). (E) and (F) Typical histograms of experimental rupture force distributions for two different pulling velocities v (7). After eliminating all the experimental force extension curves with clearly visible multiple bond signatures as those in (B) and (C), the number of remaining “apparent single bond rupture events” contributing to (E) was 202, and 151 for (F). The main features are a pronounced first peak (most probable rupture force), vague indications of possible secondary peaks, and a “long tail”.

Figure 2:

(A) Schematic sketch of dynamic force spectroscopy by AFM: a chemical bond of interest, e.g. in a ligand-receptor complex, is connected via two linker molecules with the tip of an AFM cantilever and a piezoelectric element at distance s . The latter is employed for “pulling down” the attached linker molecule at some constant velocity v which in turn leads to an elastic reaction force $F(s)$ of the cantilever, determined from the deflection of a laser beam. (B) Illustration of the model for multiple parallel bonds. The AFM tip is modeled as a half sphere and forces \mathbf{f}_i act on the ligand-receptor bonds.

Figure 3:

The dashed lines exemplify six realizations of force extension curves for double bonds ($N = 2$), numerically simulated as described in Sect. 2. Receptors were uniformly distributed on the sample surface with density $\rho_{\text{rec}} = 10^{-3} \text{ nm}^{-2}$. For a better comparability with the experimental curves from Figs. 1A-D, we sampled the force extension curves in regular time steps of $\Delta t = 0.1 \text{ ms}$ and added a Gaussian (thermal) noise with standard deviation $\sigma_f = \sqrt{\kappa k_B T} = 6.4 \text{ pN}$ (2). After that, a running average over 0.5 ms was calculated, imitating the effect of an experimental low pass filter, and resulting in the solid lines. The distance Δs between the rupture of the two bonds is indicated in each figure. The dotted line in the bottom right panel exemplifies one realization of a force extension curve for a single bond ($N = 1$, cf. Fig. 1A). The somewhat larger fluctuations observed in Figs. 1A-D can be attributed to instrumental noise on top of the thermal noise.

Figure 4:

(A) Red: Probability of formation (and rupture) of at least one bond (i.e. $N \geq 1$) within one force distance cycle. Black: Probability of observing a “false single bond” (i.e. an apparent single bond is *de facto* a (hidden) multiple bond). Blue: Fraction of “false single bonds” among all multiple bonds. All three probabilities are presented for various values of the density ρ_{rec} of uniformly distributed receptors and have been obtained as detailed in Sects. 2 and 3. The error bars indicate the statistical spread (standard deviation) due to our sampling of 100 different tips (see main text). (B) The corresponding mean rupture forces $\langle f \rangle$. (C) Representative rupture force distribution for one AFM tip (see main text) and $\rho_{\text{rec}} = 2 \cdot 10^{-4} \text{ nm}^{-2}$. (D) Same for $\rho_{\text{rec}} = 10^{-3} \text{ nm}^{-2}$.

Figure 5:

Same as Figs. 4 (A) and (B), but for $N_{\text{lin}} = 5$ linkers in (A) and (B), and $N_{\text{lin}} = 15$ linkers in (C) and (D).

Figure 6:

(A) Fraction of “false single bonds” among all multiple bonds versus resolution limit Δs_{\max} for maximum binding lengths $d_{\max} = 8$ nm (solid), $d_{\max} = 12$ nm (dotted), and $d_{\max} = 16$ nm (dashed). For further details regarding the employed receptor clustering model see main text. (B) Probability of observing a “false single bond” (i.e. an apparent single bond is *de facto* a (hidden) multiple bond). (C) Rupture force distributions for $\Delta s_{\max} = 1$ nm. For reasons of better visibility, the distribution for $d_{\max} = 12$ nm is not shown.

Figure 7:

(A)-(D) Rupture force distributions for different pulling velocities v , assuming clustering of receptors. For further simulational details see main text. (E) The corresponding survival probabilities according to Eq. 11. Velocities increase in the direction indicated by the arrow. (F) The most probable rupture force f^* from (A)-(D) versus logarithm of the loading rate λ . The solid line shows the best linear fit. For more details see main text.

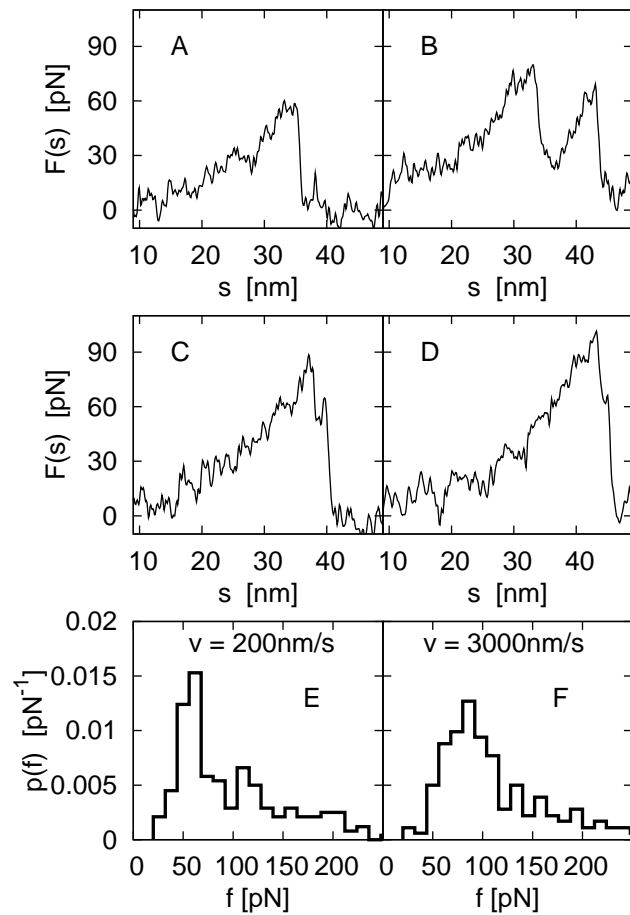


Figure 1:

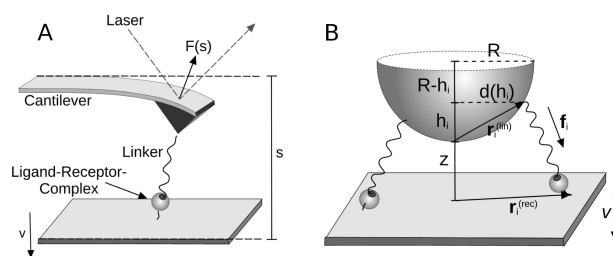


Figure 2:

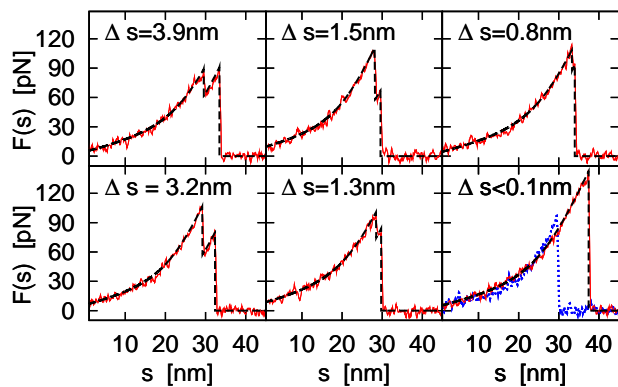


Figure 3:

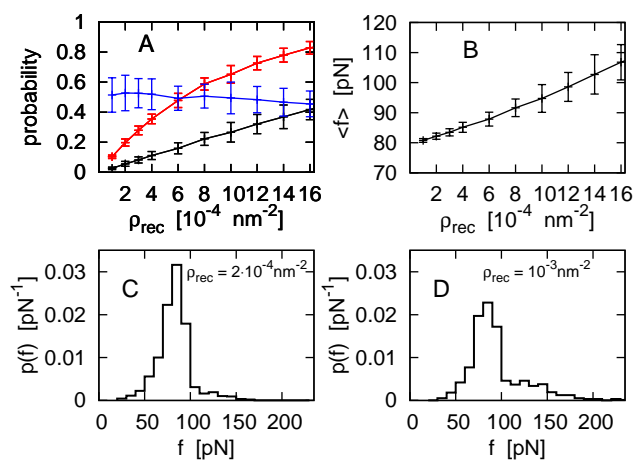


Figure 4:

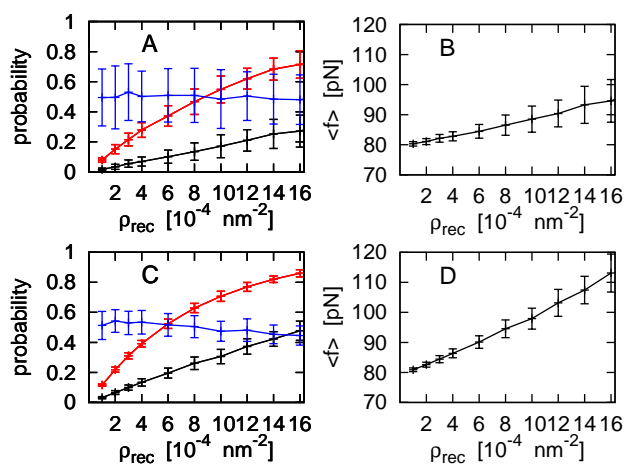


Figure 5:

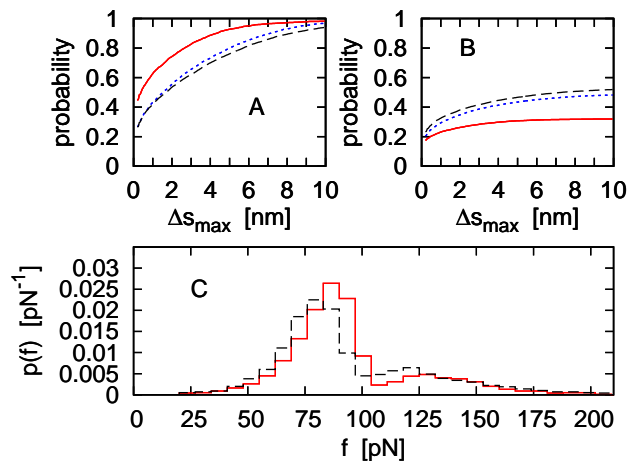


Figure 6:

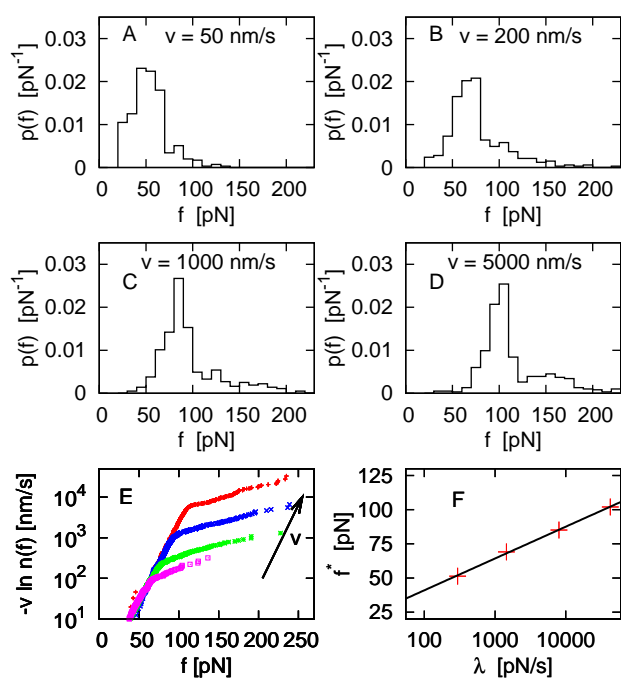


Figure 7: